ACS OMEGA

http://pubs.acs.org/journal/acsodf

Article

Inkjet Printing of a Benzocyclobutene-Based Polymer as a Low-k Material for Electronic Applications

Filippo Iervolino,* Raffaella Suriano, Martina Scolari, Ilaria Gelmi, Laura Castoldi, and Marinella Levi

Cite This: *ACS Omega* 2021, 6, 15892−15902

Read Online

ACCESS | Metrics & More | Article Recommendations | Supporting Information

ABSTRACT: Polymeric materials with a low dielectric constant are widely used in the electronic industry due to their properties. In particular, polymer adhesives can be used in many applications such as wafer bonding and three-dimensional integration. Benzocyclobutene (BCB) is a very interesting material thanks to its excellent bonding behavior and dielectric properties. Usually, BCB is applied by spin-coating, although this technology does not allow the fabrication of complex patterns. To obtain complex patterns, it is necessary to use a printing technology, such as inkjet printing. However, inkjet printing of BCB-based inks has not yet been investigated. Here, we show the feasibility of printing complex patterns with a BCB-based ink, reaching a resolution of 130 μm. We demonstrate that with a proper dilution, BCB-based inks enter the printability window and drop ejection is achieved without the formation of satellite drops. In addition, we present the conditions in which there is an appearance of the coffee ring effect. Inks that feature a too high interaction with the substrate are more likely to show the coffee ring effect, deteriorating the printing quality. We also observe that it is possible to achieve a better film uniformity by increasing the number of printed layers, due to redissolution of the BCB-based polymer that helps to level possible inhomogeneities. Our work represents the starting point for an in-depth study of BCB-based polymer fabrication using jet printing technologies, as a comparison of the bonding quality obtained with different materials and different technologies could give more information and broaden the perspective regarding this field.

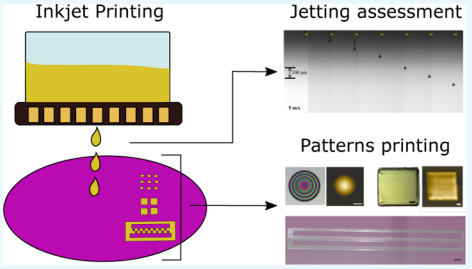

INTRODUCTION

Polymer dielectric materials have gained a lot of interest in the electronic industry in the last decade. In particular, polymers having a low dielectric constant (k) are fundamental for applications such as interlayer dielectrics (ILD), wafer bonding, three-dimensional (3D) integration, and packaging.[1,2] A low-k material is necessary to minimize the resistance−capacitance (RC) delay, the crosstalk, and the power dissipation.[3] Benzocyclobutene (BCB)-based polymers are very interesting polymers for the abovementioned applications. The BCB-based polymer is a thermoset polymer adhesive that features a very low k (~2.65 for the frequency range 10 Hz to 1 MHz[4]), reduced copper diffusion and moisture absorption, an excellent planarization, and high resistance to chemicals.[2,5−10] Its excellent adhesion properties toward silicon (Si) made it suitable for wafer bonding and 3D integration.[11,12] The BCB-based polymer is usually processed as a solvent-based thermoset polymer. First, the solution is applied to the Si wafer, then the solvent is allowed to evaporate, and finally the BCB-based polymer is cured by heating. Solvent-based thermoset polymers are of particular interest due to their relatively low viscosity.[13] The low viscosity is due to the presence of the solvent that reduces the viscosity while increasing the dilution.[14] Moreover, before curing, the polymers in the solution are made by monomers and oligomers that have a relatively low molecular weight and help to keep the viscosity low.[14,15] The relatively low viscosity of solvent-based polymers is important for technologies that cannot process materials having a high viscosity. For example, moderate and low levels of viscosity are required for gravure printing and jet printing, respectively.[16] Spray coating technologies require the use of low-viscosity polymer as well, in the range 0.05−0.1 Pas.[14] The most used technology for this application is spin-coating. Spin-coating has the advantage of obtaining very thin and uniform films. In addition, it is not expensive, fast, and simple.[17] However, the main disadvantage is the impossibility to apply the polymer adhesive following a specific pattern. To achieve patterning on a substrate, a lithographic process is necessary, which dramatically increases the time and cost of the process.[18] Moreover, this technology is characterized by material wastes and by the impossibility of using it when high topographies are present.[19,20] Technologies that are able to overcome the aforementioned issues are the so-called printing techniques. Among all the printing technologies, one of the most recent is inkjet printing. Inkjet printing is based on the selective emission of drops of an ink, which is a

Received: March 19, 2021
Accepted: May 14, 2021
Published: June 10, 2021

solution containing the functional material, the solvent, and possible additives. Two different inkjet printing technologies exist: continuous inkjet (CIJ) and drop-on-demand. The main advantage of the drop-on-demand technique over the CIJ is the possibility of obtaining drops with a smaller diameter, which allows printing features with a higher resolution.[21,22] Thus, the drops generated with the CIJ system have a diameter of ∼100 μm, while the drops obtained using a drop-on-demand system can reach diameters down to 20 μm.[23,24] The reason for the difference in the drop size lies in the different drop generation system, which produces drops larger than the nozzle size for the CIJ system.[24−26] Furthermore, the drop-on-demand system allows further reducing the drop sizes managing the ejection parameters.[24] For the drop-on-demand systems, one method to achieve drop ejection is a piezoelectric actuation. A piezoelectric element, surrounding the ink reservoir, is deformed by the application of a voltage. The deformation applies a pressure to the ink reservoir causing the ejection of the drops.[21,25] However, inkjet printing technology has some major drawbacks. First, the viscosity of printable inks is very limited, being at maximum tens of mPas.[23] This is a major issue for the ink formulation, because a high dilution is necessary in order to have printable inks. Furthermore, ink properties and printing parameters are crucial for optimal drop ejection and for avoiding splashing or satellite drop formation. The second main issue is the coffee ring effect, also called the coffee stain effect.[27−36] It is due to the accumulation of nonvolatile species at the edge of the drop as an effect of the evaporation of the solvent, forming a ring-like shape.[37] The coffee ring effect occurs when the particles of the nonvolatile solute present in the ink pin to the substrate at the edge of the drop, while a capillary flow occurs from the center of the drop toward the edge, transporting the solute.[23,38] Several solutions have been found to avoid or control the coffee ring effect: proper choice of the solute particles (i.e., ellipsoidal shape),[39] a bigger dimension of the solute particles,[40] reducing substrate temperature,[41,42] use of appropriate additives and surfactants,[37,43] and inducing the Marangoni flow, which is driven by an interfacial surface tension gradient caused by the presence of two solvents with different boiling temperatures.[44] In the literature, many works can be found on the inkjet printing of polymeric inks.[45−62] Bernasconi et al.[45] printed SU8-based inks on a Si wafer substrate. They were able to print complex patterns to be used as masks for metal electrodeposition. Moon et al.[56] studied the morphological features of printed SU8 for the fabrication of a fully printed organic field effect transistor. Robin et al.,[49] instead, investigated the inkjet printing of epoxy-based inks. The authors evaluated the formation of coffee ring effect by studying different printing parameters, such as the substrate temperature and the spacing between two adjacent drops. Inkjet printing of polymer adhesives for application in electronic has also been investigated in the literature.[63−65] Miskiewicz et al.[63] proved the feasibility of using inkjet printing to fabricate packaging architectures made of a polymer dielectric. Roshanghias et al.,[64] instead, examined UV, thermal, and hybrid curable polymer adhesives for the packaging of micro-opto-electro-mechanical systems. Hamad et al.[65] used inkjet printing to deposit UV-curable poly(4-vinylphenol-*co*-methyl methacrylate) to bond a polymer-based microfluidic system. To our knowledge, inkjet printing of a BCB-based polymer has not yet been studied or proposed in the literature, despite being a well-known dielectric material in the electronic industry.

Therefore, we propose the first study on the inkjet printing of BCB-based inks as a viable fabrication technology for patterned complex structures. In this work, we focused first on the characterization of inks, their printing, and jetting assessment. Then, we investigated the morphology of BCB-printed patterns. Finally, we proved the feasibility of printing complex patterns.

RESULTS AND DISCUSSION

Ink Printability. Different inks were prepared and their printability was evaluated. First, the material as purchased was studied, that is, Cyclotene resin. Cyclotene is a polymer solution containing BCB-based polymer dissolved in 1,3,5-trimethylbenzene, also known as mesitylene (MES). Thermogravimetric analysis showed that the content of the BCB-based polymer in the solution was 48 wt % (Figure S1). The ink featured a viscosity of 52 mPas at 25 °C, which was higher than the theoretical limit for drop ejection for a Dimatix disposable cartridge, set as ∼30 mPas. Therefore, a dilution of the BCB-based polymer was performed to lower the viscosity. Based on the preliminary printing tests, we chose a BCB-based polymer concentration of 25 wt % and we kept this concentration fixed for the two inks we studied. Two different solvents were used to perform the dilution: MES and a MES−di(propylene glycol) dimethyl ether (DPGDME) mixture. Table 1 reports

Table 1. Ink Formulations Used in This Work and Their Composition

ink formulation	BCB wt fraction	MES wt fraction	DPGDME wt fraction	total solvent wt fraction
Cyclotene	0.48	0.52	0	0.52
BCB/MES	0.25	0.75	0	0.75
BCB/MES−DPGDME	0.25	0.28	0.47	0.75

all the studied concentrations and compositions. Thanks to the dilution, it was possible to reach a viscosity of 5 and 6.5 mPas using MES and MES−DPGDME solvents, respectively. Furthermore, all the inks showed a Newtonian behavior in the shear rates of interest (Figure S2).

A detailed study on the printability was carried out using the well-known Reynolds (Re), Weber (We), Ohneserge (Oh), and inversed Ohneserge (Z) adimensional numbers, which are reported in eqs 1−4

$$Re = \frac{v\rho D_n}{\eta} \tag{1}$$

$$We = \frac{v^2\rho D_n}{\gamma} \tag{2}$$

$$Oh = \frac{\sqrt{We}}{Re} = \frac{\eta}{\sqrt{\gamma\rho D_n}} \tag{3}$$

$$Z = \frac{1}{Oh} = \frac{\sqrt{\gamma\rho D_n}}{\eta} \tag{4}$$

where v is the ejection velocity of the drop, D_n is the diameter of the nozzle of the cartridge, ρ is the density of the ink, η is the dynamic viscosity of the ink, and γ is the surface tension of the ink. Table 2 shows the properties of the inks and the relative adimensional number values at different printing speeds. It is important to notice that Oh and Z numbers are

https://doi.org/10.1021/acsomega.1c01488
ACS Omega 2021, 6, 15892−15902

Table 2. Ink Properties, Printing Speed, and Values of Adimensional Numbers for Each Studied Ink

ink	ρ (g/cm^3)	η (mPas)	γ (mN/m)	v (m/s)	*Re*	*We*	*Oh*	*Z*
Cyclotene	0.95	52	29.15	3	1.15	6.15	2.15	0.46
				5	1.92	17.08		
				7	2.68	33.48		
BCB/MES	0.91	5	28.64	3	11.47	6.01	0.21	4.68
				5	19.11	16.7		
				7	26.75	32.74		
BCB/MES−DPGDME	0.93	6.6	26.83	3	8.88	6.56	0.29	3.47
				5	14.8	18.22		
				7	20.71	35.71		

not affected by the ejection velocity, meaning that they represent an indication of the printability of the ink based only on the ink's physical properties, that is, density, surface tension and viscosity, and on the nozzle diameter. Many works in the literature affirm that inks with a *Z* value between 1 and 10 are printable.[25,66] If $Z < 1$, it means that the ink is too viscous and that there is not enough energy for drop formation. However, if $Z > 10$, formation of satellite drops begins. From our results, it is possible to observe that Cyclotene ink presented a *Z* value lower than 1, meaning that it is too viscous to be printed. After dilution with the two different solvents, the obtained inks featured a *Z* value in the printable range, being 4.68 and 3.47 for the BCB/MES and the BCB/MES−DPGDME ink, respectively. Although properly tuning the Z value is necessary, it is not enough to achieve a stable drop ejection. Indeed, potential inertial contributions need to be considered to avoid the formation of satellite drops or splashing. For this reason, further considerations should be performed on the *We* number because it relates the inertial forces to the surface tension of the ink.[54] Liu and Derby[67] stated that a printable ink featuring the formation of stable drops should have a *We* number between 2 and 25. Below 2, there is no drop ejection and above 25, there is the formation of satellite drops.

Figure 1 shows the *We* versus *Z* printability diagram of the studied ink showing the boundaries found by Liu and Derby[67] at three different ejection speeds, that is, 3, 5, and 7 m/s. It is also possible to observe that if $Z < 40$, a higher value of *We* is necessary to achieve ejection (represented by the diagonal dashed line). However, if $Z > 5$, a lower value of *We* is needed to have the formation of satellite drops. In addition, the *Z* versus *We* printability diagram was used to estimate the most appropriate drop ejection speed for our inks. According to the printability diagram, the optimal speed was 5 m/s. Higher speeds, such as 7 m/s, entered in the satellite drop formation region, while 3 m/s represented the limit at which drop ejection occurred.

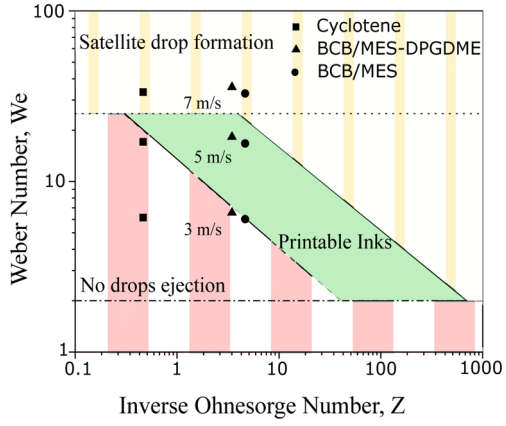

Figure 1. *Z* vs *We* printability diagram of Cyclotene, BCB/MES, and BCB/MES−DPGDME inks at three different ejection speeds. The graph highlights three different regions: the region of no drop ejection (large stripes fill), the printability range (solid fill), and the region of formation of satellite drops (small stripes fill). From the graph, it was possible to individuate the most suitable speed for the ejection of the inks, which is 5 m/s.

To verify the ideal ejection speed, the ejection of drops from the nozzle at 3, 5, and 7 m/s was monitored with a stroboscopic camera. The ejection at different speeds was obtained modifying the maximum applied voltage of the pulse. The maximum applied voltages were 12, 15, and 22 V for achieving a speed of 3, 5, and 7 m/s, respectively (Figure S3). An appropriate ejection speed is essential for achieving good printing quality. It is necessary to avoid the formation of satellite drops and that the drop keeps a spherical shape after ejection. Figure 2 shows the time-lapse of the drop ejection over 90 μs for the aforementioned speeds using the BCB/MES ink.

Results highlighted that a speed of 7 m/s caused the formation of satellite drops. The satellite drops were not reincorporated into the main drop, which is deleterious for the printing quality A speed of 3 m/s, instead, is very close to the lower speed limit of the ink, which could cause a nozzle clogging due to an insufficient energy for the emission of the drops over long printing times. Even though nozzle clogging does not occur, the drop fall might be unstable, not following a straight line. Therefore, we chose 5 m/s as the ideal ejection speed. The formation of a single stable drop was observed and no nozzle clogging was reported for long printing times. In addition, the drops kept a spherical shape during the entire fall.

Single-Drop Array. A 5 mm × 5 mm drop array was printed on a SiO_2 substrate to study the morphology of a single printed drop, that is, the minimum printable feature. Each drop was printed with a drop spacing of 250 μm, to avoid any possibility of overlapping. Figure 3a,b shows the images taken with a microscope of drop arrays printed with the BCB/MES and the BCB/MES−DPGDME ink, respectively. The drops printed with the BCB/MES ink showed a splat diameter (i.e., the diameter of the drops deposited on the substrate) of ∼60 μm and a spherical shape, with the absence of the coffee ring effect. While, the drops printed with the BCB/MES−DPGDME ink had a diameter of ∼120 μm and they exhibited a significant coffee ring effect. The reason for the difference in the morphology and the diameters of the drops needs to be linked to the different interactions with the SiO_2 substrate. Figure 3c,d shows pictures taken during contact angle measurements for BCB/MES and BCB/MES−DPGDME

https://doi.org/10.1021/acsomega.1c01488
ACS Omega 2021, 6, 15892−15902

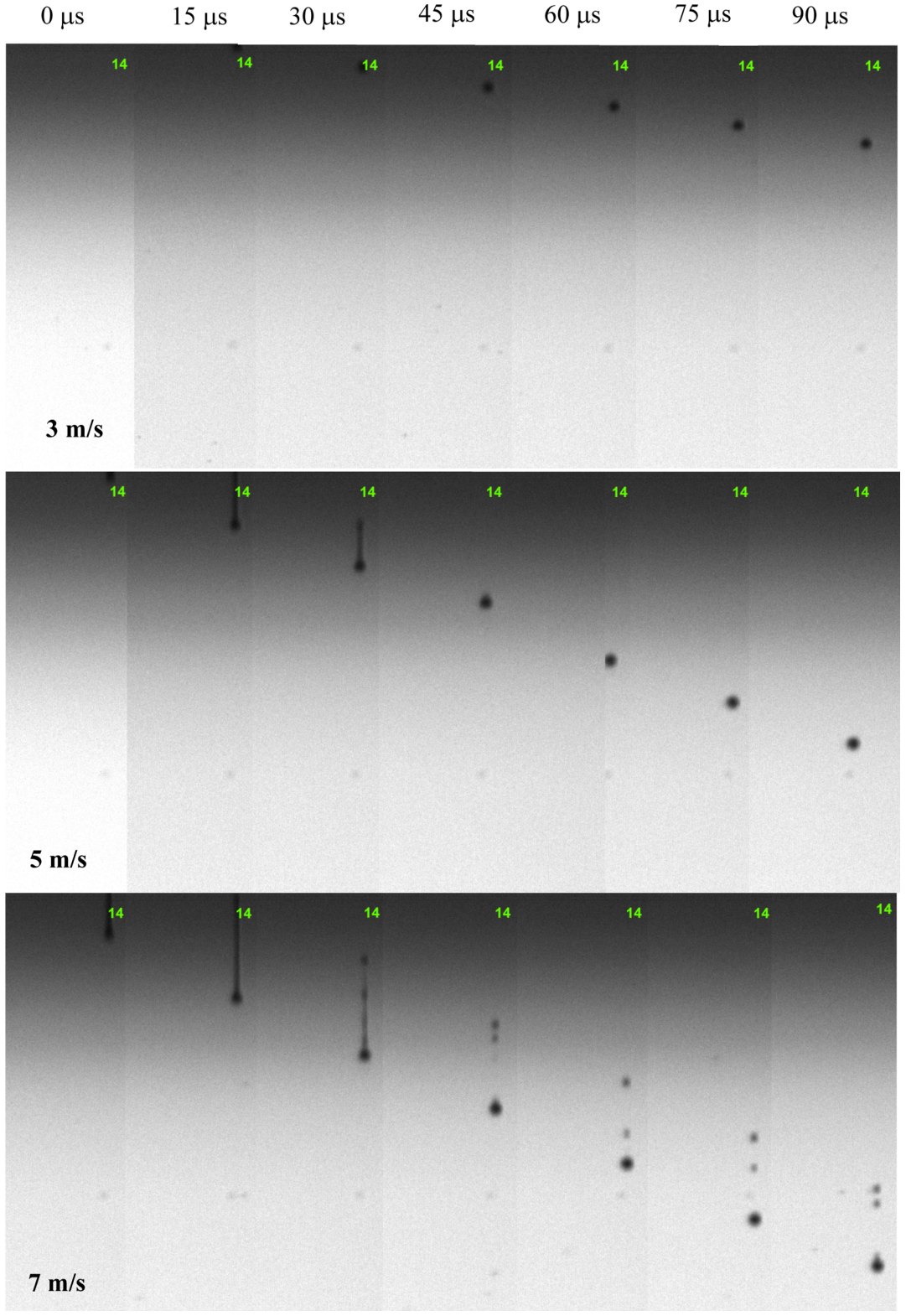

Figure 2. Time-lapse of 90 μs of the drop ejection from the nozzle using the BCB/MES ink at three different speeds: 3, 5, and 7 m/s. The time delay from each picture is 15 μs. The pictures highlight that 5 m/s is the optimal ejection speed. The formation of satellite drops is observed at 7 m/s, while ejecting at 3 m/s was too close to the lower threshold speed limit.

inks, respectively. BCB/MES ink exhibited a higher contact angle than BCB/MES−DPGDME. The measured value for the BCB/MES ink was ∼15°, while for the BCB/MES−DPGDME ink the real contact angle was lower than the minimum angle detectable by the equipment, therefore we can conclude that the contact angle was lower than 5°. We think that the reason for the different interaction with the substrate relies on the chemical structure of DPGDME, which creates polar interactions with the SiO_2 substrate. Therefore, inks containing DPGDME had a higher interaction with SiO_2, leading to a

https://doi.org/10.1021/acsomega.1c01488
ACS Omega 2021, 6, 15892−15902

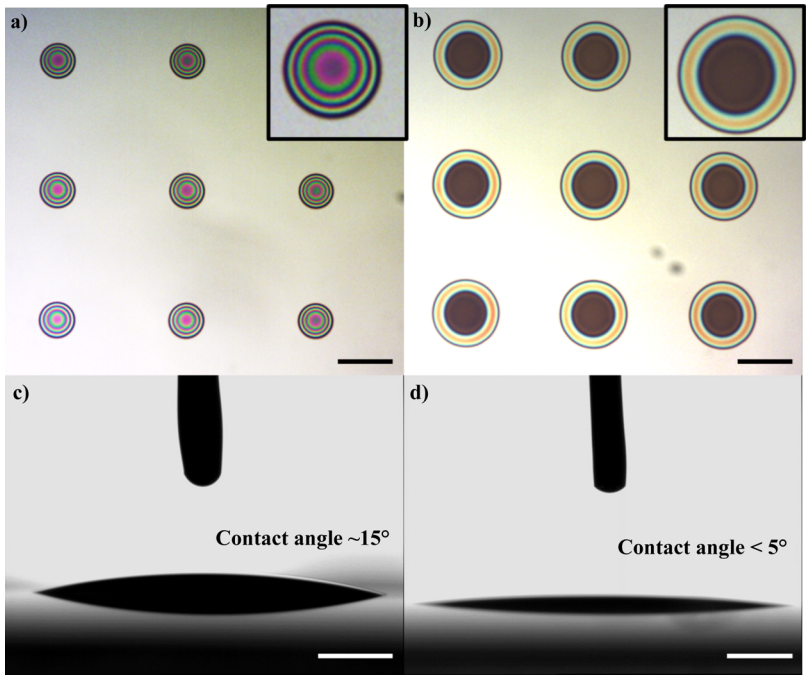

Figure 3. (a,b) Images taken using a microscope with a 5× magnification of the drop array of (a) BCB/MES and (b) BCB/DPGDME inks. In the box on the top right corner, a magnified view of one drop is reported. It is possible to observe the formation of the coffee ring effect for BCB/MES−DPGDME drops. Scale bars measure 100 μm. (c,d) Images taken during the contact angle measurements of (c) BCB/MES and (d) BCB/DPGDME inks. The BCB/MES−DPGDME ink showed much lower contact angle values, explaining the formation of the coffee ring effect for this ink. Scale bars measure 1 mm.

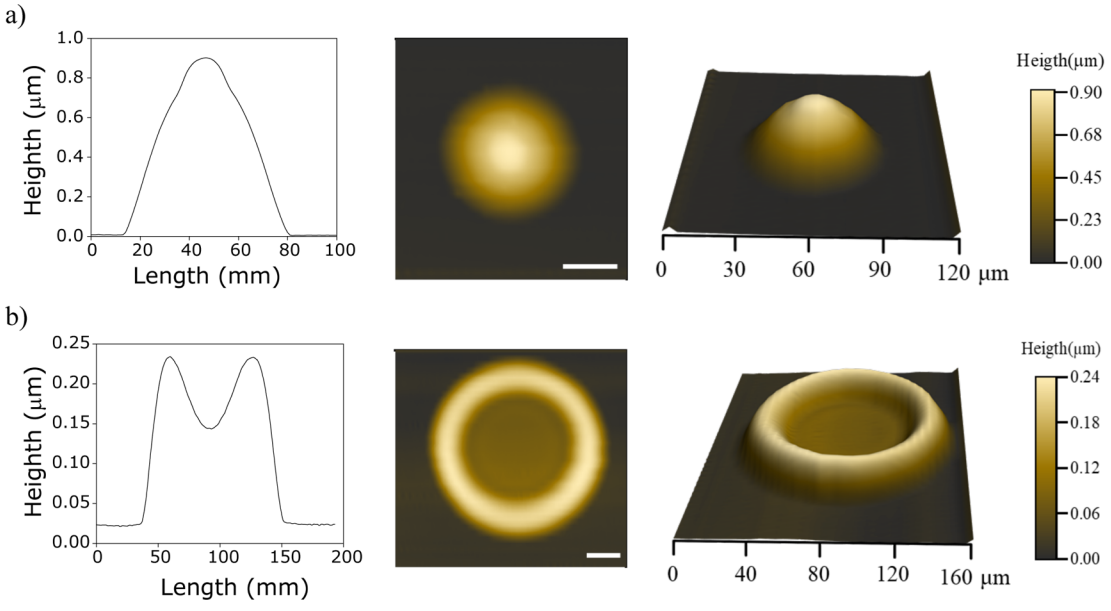

Figure 4. 1D, 2D, and 3D profilometry analyses of a single drop printed on a SiO_2 substrate for (a) BCB/MES ink and (b) BCB/MES−DPGDME ink. It is possible to observe the formation of the coffee ring effect for the BCB/MES−DPGDME ink. Scale bar measures 25 μm.

lower contact angle. Consequently, a lower contact angle led to a higher splat diameter. Knowing the value of the splat diameter is fundamental for two reasons. First, it allows us to know the maximum resolution of the ink and to choose the most suitable drop spacing. Second, the value of the splat diameter is directly correlated with the appearance of the coffee ring effect. There is a threshold value for the splat diameter above which the coffee ring effect is observed, while below the threshold value the drop takes a cap-like shape.[29]

Therefore, it is fundamental to choose an ink with a sufficiently high contact angle on the substrate of interest to maximize the resolution of the print and to avoid possible printing defects due to the coffee ring effect. As a matter of fact, the cap-like shape has to be preferred over the ring-like shape. The cap-like shape is generated by the surface tension of the drop itself, while the ring-like shape is due to a material transport phenomenon, which may cause print defects and surface inhomogeneities.[29] Profilometry measurements were

https://doi.org/10.1021/acsomega.1c01488
ACS Omega 2021, 6, 15892−15902

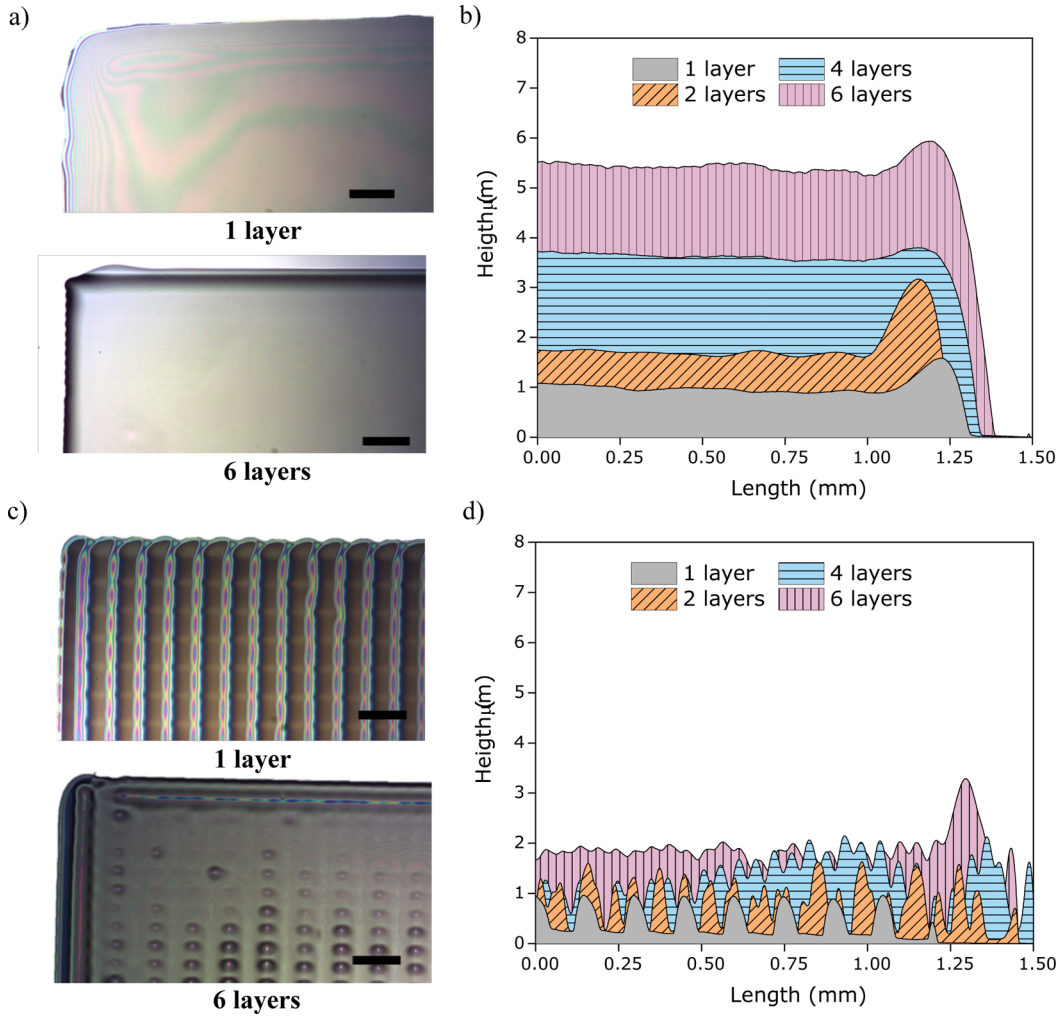

Figure 5. (a) Optical microscopy of the one-layer and six-layer squares printed with the BCB/MES ink. (b) Stick profilometry of the one-, two-, four-, and six-layer squares printed with the BCB/MES ink. (c) Optical microscopy of the one-layer and six-layer squares printed with the BCB/MES−DPGDME ink. (d) Stick profilometry of the one-, two-, four-, and six-layer squares printed with the BCB/MES−DPGDME ink. The BCB/MES ink showed a better film quality thanks to the absence of the coffee ring effect. Scale bars measure 100 μm.

conducted on the printed single drops to estimate quantitatively their height and to visualize their profile. Figure 4a,b shows the one-dimensional (1D), two-dimensional (2D), and 3D profilometry analysis of the BCB/MES and BCB/MES−DPGDME printed drops, respectively. The measurements confirmed the observation made by optical microscopy. Consequently, no coffee ring effect was observed for the BCB/MES drop, which featured a cap-like shape. The height of the drop gradually increased going toward the center of the drop, until a maximum height of 0.9 μm was reached. Regarding the BCB/MES−DPGDME drop, the 1D analysis showed that the highest point of the drop profile was obtained at the border of the drop due to a strong material agglomeration, while a depletion of material at the center can be observed, proving the appearance of the coffee ring effect. The height difference between boundaries and central region was about 0.12 μm, with the highest measured value of 0.2 μm. 2D and 3D analyses showed clearly the ring-like shape typical of the coffee ring effect and the material agglomeration toward the border of the drop.

Square Array. A 2 × 2 square array was printed to evaluate the morphology and the quality of films. Figure 5a,b shows the images obtained through an optical microscope and the 1D profilometry analysis of the squares printed with the BCB/MES ink. The squares were printed varying the number of layers from one to six. From the optical microscopy images, it is possible to observe that an overall uniform print was obtained. However, the one-layer print exhibited some inaccuracy at the edges of the square, probably due to the solvent evaporation. In addition, an accumulation of material toward the edges was observed as well. Even though the BCB/MES ink did not present the coffee ring effect, some transport of material during drying still occurred. This could be related to the morphology of the drying material, which is no more represented by a single small drop, but by a larger amount of material that favors capillary flow. We observed that increasing the number of layers, the overall film quality increased, especially at the edges. In addition, the accumulation of material at the edges of the squares was reduced for the four-layer and six-layer prints. The beneficial effect of printing with multiple layers can be explained by the fact that when a new layer is printed, a partial redissolution of BCB-based polymer occurs. The redissolution helped to accommodate print defect and covered possible material depletion. The thickness measured at the center of the printed squares was 1.0, 1.7, 3.8, and 5.5 μm for the one-, two-, four-, and six-layer print,

https://doi.org/10.1021/acsomega.1c01488
ACS Omega 2021, 6, 15892−15902

respectively. Therefore, a successful addition of material was observed each time the number of layers was increased. However, the increase in the thickness of the prints was not linearly dependent on the number of printed layers. This can be explained again by the abovementioned material transport and redissolution effects. The two-layer print is just 0.8 μm thicker at the center than the one-layer print. This is explained by the strong accumulation of material that occurred at the edge, where an increase from 1.5 to 3.2 μm was observed. The four-layer print, instead, showed just a 0.7 μm increase of the thickness of the outer region of the square thanks to the redissolution phenomenon. While at the center of the print, where the material replenished, an increase of 2.1 μm was observed.

Figure 5c,d shows the images obtained through an optical microscope and the 1D profilometry analysis of the squares printed with the BCB/MES−DPGDME ink. In this case, the morphology of the printed squares is very irregular. The one-layer print clearly showed each printed line, meaning that coalescence of the drops occurred just along the printing direction. This effect is probably related to the coffee ring effect, which caused strong material accumulation at the border of each printed line. Printing multiple layers had still a beneficial effect, reducing the coffee ring effect, but did not completely overcome the issue. The six-layer square showed an irregular morphology, with regions showing material depletion. In this case, the irregularities caused by the coffee ring effect were too big to be recovered by the BCB-based polymer redissolution. In addition, the height measured at the center of the print achieved by the six-layer print was ~2 μm, much lower than 5.5 μm obtained with the BCB/MES ink. The lower profile thickness is attributed to the higher splat diameter and the lower height of the BCB/MES−DPGDME ink drops, compared to the BCB/MES drop (Figure 4).

We were also interested in evaluating the overall surface morphology of film-like prints. For this reason, we printed an array of squares with a 750 μm edge for the BCB/MES ink and we performed 2D and 3D profilometries. Figure 6 shows the microscopy images, the 2D and 3D profilometries of the 750 μm squares printed with one, two, four, and six layers. All the prints showed an accumulation of material to the right edge, while a depletion of material was present on the left edge. The darker regions are the ones with a lower height, therefore presenting a material depletion, while the brighter ones have a higher height, indicating the presence of material accumulation. The reason for the different behavior can be explained by the way the squares were printed.

The first printed line was the one at the right, while the last one was at the left. It means that when the last line is printed, the material transport phenomenon responsible for the material accumulation already happened, resulting in a material depletion in that region. This phenomenon is particularly emphasized for the one- and two-layer prints because the BCB-based polymer redissolution that helps material redistribution was still not predominant. For the four- and six-layer prints, we observed a higher film uniformity due to a lower material accumulation and depletion toward the border of the squares.

Bonding Pattern. After completing the evaluation of the print quality and morphology on simple patterns, we printed complex patterns with the presence of small features. The geometry is a real bonding pattern used in the semiconductor industry. Figure 7a,b shows a picture of the printed bonding pattern featuring a dimension of 5.5 mm × 11.5 mm and 5.5

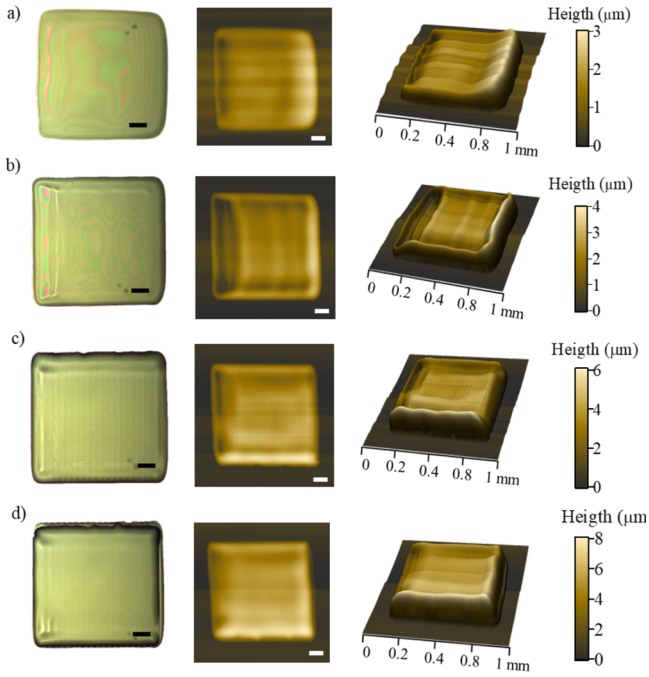

Figure 6. Optical microscopy images and 2D and 3D profilometry of a square featuring a 750 μm edge printed using the BCB/MES ink with (a) one layer, (b) two layers, (c) four layers, and (d) six layers. Scale bars measure 100 μm.

mm × 45.5 mm, respectively. The prints were performed to assess the feasibility of printing complex patterns of relatively large dimensions. Figure 7c shows the 2D sketch of the bonding pattern and also presents a magnified view of two regions of the pattern. In addition, the images taken using the microscope of the abovementioned regions were reported. By design, the minimal feature of the pattern was 130 μm, while the cavities that were present had a dimension of 224 μm × 208 μm. The pattern was printed using the BCB/MES ink with four layers because the four-layer print was the one showing the best compromise between the film quality, film thickness, and dimension accuracy. Figure S4 shows the microscopy image of the central region of the pattern printed with one, two, four, and six layers. It is shown that increasing the number of layers until four layers had a beneficial effect on the film quality and dimension accuracy. Instead, the six-layer pattern started to show a worsening of the dimension accuracy. This is probably due to the presence of small features that have been negatively affected by the presence of a higher number of layers. Regarding the two regions of the pattern that are reported, the first one is the left portion, featuring a width of 614 μm. We observed that the print reproduced with precision the feature of the designed pattern. The width of the printed pattern was 640 μm, showing a difference of just 30 μm from the design value. Also, the internal corner was reproduced faithfully with good quality. The only defect is present at the outer edge (the last printed line), which showed a slightly wavy shape due to incomplete drop coalescence localized only at this point. The second region we showed was the central one, which is the most critical due to the presence of small features and cavities.

The printed pattern showed also in this case a faithful representation of the designed pattern. For the measurement from II to V, the maximum measured differences between the designed and printed pattern were 15 and 21 μm, respectively.

https://doi.org/10.1021/acsomega.1c01488
ACS Omega 2021, 6, 15892−15902

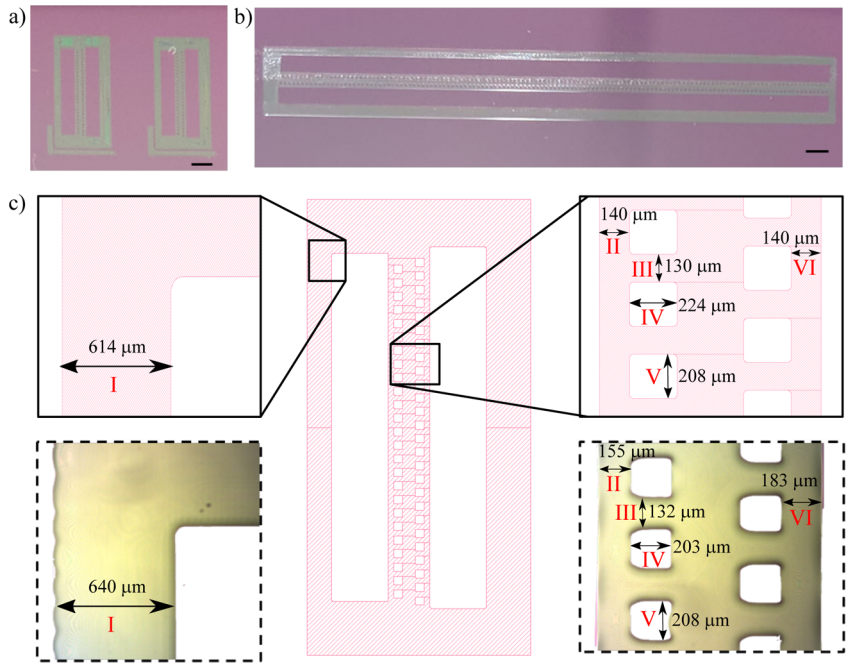

Figure 7. (a,b) Microscopy images of the bonding pattern measuring (a) 5.6 mm × 11.5 mm and (b) 5.6 mm × 45.5 mm printed with the BCB/MES ink. Scale bars measure 2 mm. (c) Schematics of the bonding pattern and two details and comparison with the actual pattern printed with the BCB/MES ink. The roman numbers represent the numbering of the measured distances. It is possible to observe that the printed patterns reproduce faithfully the dimensions of the design.

The region showing the lower level of accuracy was the one on the right, corresponding to measure VI. Here, the difference between the printed and the designed features was 43 μm. In this case, the lower level of accuracy can be explained by an excessive spreading of the print. Overall, the aforementioned results showed the feasibility of printing complex patterns of large dimensions with a faithful reproduction of details imposed by the design.

CONCLUSIONS

In this paper, we showed for the first time the inkjet printing of BCB-based inks for applications in the electronic industry. The study on the printability of the inks showed that an appropriate choice of the ejection speed is fundamental to achieve good printing quality. A too low speed might result in incomplete ejection, while a too high speed led to the formation of satellite drops. The optimal ejection speed for our inks was 5 m/s. The interaction with the substrate was evaluated for the two printable inks, creating an array of isolated drops. The prints showed the formation of the coffee ring effect for the BCB/MES−DPGDME ink. This was due to the lower contact angle showed by this ink toward the SiO_2 substrate, leading to the formation of drops with a higher diameter and thus to the appearance of the coffee ring effect. The square array allowed us to evaluate the effect of using different numbers of layers. Results showed that, in the case of BCB/MES ink, printing multiple layers had a beneficial effect on the film morphology thanks to a partial BCB-based polymer redissolution. Instead, the BCB/MES−DPGDME ink showed a very irregular morphology caused by the excessive coffee ring effect that caused partial accumulation of material. This proved the importance of tuning the ink properties to avoid the appearance of the coffee ring effect. The strong inhomogeneities caused by the material agglomerations and depletions are detrimental to the film quality and, therefore, should be avoided. Finally, a real bonding pattern was printed with the BCB ink to show the feasibility of printing complex shapes. The results showed that it was possible to print features with dimensions down to 130 μm. The metrology performed on the printedpattern highlighted that the features on the printed pattern are faithful representation of the designed pattern.

In conclusion, BCB-based inks can be used to fabricate complex patterns with small features through inkjet printing technology. Future works will be focused on the characterization of the electrical and adhesive properties of inkjet-printed manufactures. The abovementioned properties will be evaluated also on the BCB-based polymer printed in an electronic device. Furthermore, we will investigate the use of different printing technologies, such as aerosol jet printing, which could overcome some drawbacks related to the drop drying and coalescence. In addition, the bonding quality of our pattern will be evaluated and compared with more traditional technologies.

METHODS

Ink Preparation. Cyclotene 3022-46 resin was purchased from Dow Chemicals. The resin contained b-staged divinylsiloxane bisbenzocyclobutene dissolved in MES. Mesitylene and di(propylene glycol) dimethyl ether were purchased from Sigma-Aldrich and used to dilute the Cyclotene resin. The two studied inks were prepared with a mass concentration of BCB-based polymer equal to 25%. The solvents were added with a 3 mL pipet into the Cyclotene kept under stirring at ambient temperature. Then, the solution was kept under stirring for 5 min to ensure complete dissolution.

Ink Characterization. Different ink properties were characterized to assess their printability. Thermogravimetric analyses were performed using a Q500 thermogravimetric analyzer provided by TA Instrument. 20 mg of material were used for each test. A heating ramp from 25 to 800 °C was set at

https://doi.org/10.1021/acsomega.1c01488
ACS Omega 2021, 6, 15892−15902

a heating rate of 20 °C/min. The tests were performed under two different atmospheres: nitrogen and air. During the tests, the mass of the sample was monitored to quantify the mass concentration of the BCB-based polymer and solvent.

Rheological characterization was performed with a stress-controlled rotational rheometer Kinexus Pro+ (Malvern Panalytical). A cone-plate geometry with a radius of 40 mm was chosen. The used gap was 0.52 mm. Flow curves, that is, viscosity vs applied shear rate, were obtained by increasing the applied shear rate until a value of 400 s^{-1}. The tests were repeated three times to verify the repeatability of the measurements.

Density measurements were performed using a pycnometer with a volume of 1.179 cm^3. The inks were kept at 25 °C with the aid of a heated bath. The inks contained in the pycnometer were then weighted. By dividing the weight by the volume of the pycnometer, the density of the inks was obtained. Surface tension and contact angle measurements were performed through an OCA-15 plus purchased from Dataphysiscs.

Surface tension measurements were carried out with the pendant drop technique. The liquid to be analyzed was loaded into a Hamilton glass syringe (Nglabtech) with a volume of 0.5 mL. Then, 12 μL of the inks are ejected from a needle with a diameter of 1.65 mm until a pendant drop is formed. Afterward, the shape of the drop was analyzed optically by the OC software, and by employing the Boshforth−Adams equation, represented in eq 5, the value of interfacial surface tension was obtained

$$\frac{1}{\frac{R_1}{a}} + \frac{\sin\varphi}{\frac{x}{a}} = -a^2 g \frac{\rho}{\gamma}\frac{z}{a} + 2 \tag{5}$$

where R_1 is the curvature radius at the apex of the drop, a is the distance from the center to the apex of the drop, φ is the angle at the apex of the drop, x is the width of the drop, g is the acceleration of gravity, ρ is the density, γ is the surface tension, and z is the vertical distance from the origin. For the contact angle technique, the liquid was loaded into the same syringe. Then, a controlled amount of liquid was ejected through a needle with a diameter of 0.52 mm and deposited onto the substrate of interest, that is, SiO_2. The shape of the drop was analyzed optically and by Young's equation, shown in eq 6, and the contact angle values were determined

$$\gamma_{lg}\cos\theta = \gamma_{sg} - \gamma_{sl} \tag{6}$$

where θ is the contact angle and γ_{lg}, γ_{sg}, and γ_{sl} are the surface tension of the liquid, the surface tension of the solid, and the solid−liquid interfacial tension, respectively. A set of five measurements on two different substrates was performed.

Inkjet Printing. The inks were printed using a Ceradrop F4-Series (MGI group). The printer was equipped with a module allowing the use of Fujifilm Dimatix disposable cartridges. We used a 10 pL cartridge featuring nozzles having a diameter of 21 μm. The first step was the selection of the most appropriate waveform to eject the ink droplets from the nozzle. Because no data were available for the inks we were using, a trial and error approach was used to choose the appropriate waveform. A representation of the used waveform is present in Supporting Information (Figure S3). We found that a bimodal curve gave us the best jetting behavior. Analysis of drop diameter, speed, and trajectory was performed using Driver Ceraprinter, an in-house software program provided by the MGI group. Regarding the printing parameters, the working distance between the printhead and the substrate was kept at 1.5 mm. The printing frequency was set at 1 kHz. The printing direction was the Y-direction (i.e., keeping the printhead fixed and moving the printing chuck). The patterns that were printed were a drop pattern, a 4 × 4 square pattern, a 6 × 6 square pattern, and a complex bonding pattern. All the patterns were printed on a SiO_2 substrate.

Pattern Characterization. Surface morphology was characterized by means of optical microscopy using a Leica FTM200. The microscope was used with direct illumination and using a 5x magnification. A KLA Tencor profilometer was used to measure the profile height of the printed patterns. For each sample, the solvent has been allowed to evaporate before the test. The profilometer used a stick with a 5 μm radius tip. The scanning speed was set at 20 μm/s with a sampling rate of 20 Hz. The scans were leveled with the two-bar method to correct the artificial slope that is originated during the measurement. The applied force was 1 mg. For 3D scans, the traces distance was set as 5 μm to maximize the resolution along the Y-direction. The scans were leveled using the least square method computed on the scanned region occupied by the wafer.

■ ASSOCIATED CONTENT

Supporting Information

The Supporting Information is available free of charge at https://pubs.acs.org/doi/10.1021/acsomega.1c01488.

Thermogravimetric analysis performed on the Cyclotene commercial resin; rheological analysis performed on the Cyclotene commercial resin, the BCB/MES−DPGDME ink, and the BCB/MES ink; graphical representation of the applied waveform to obtain ejection at three different speeds: 3, 5, and 7 m/s; and detailed microscopy images of the bonding pattern printed with one, two, four, and six layers (PDF)

■ AUTHOR INFORMATION

Corresponding Author

Filippo Iervolino − *Department of Chemistry, Materials and Chemical Engineering "Giulio Natta", Politecnico di Milano, Milan 20133, Italy;* orcid.org/0000-0001-5908-9407; Email: filippo.iervolino@polimi.it

Authors

Raffaella Suriano − *Department of Chemistry, Materials and Chemical Engineering "Giulio Natta", Politecnico di Milano, Milan 20133, Italy;* orcid.org/0000-0002-7448-359X

Martina Scolari − *STMicroelectronics, Agrate Brianza 20864, Monza and Brianza, Italy*

Ilaria Gelmi − *STMicroelectronics, Agrate Brianza 20864, Monza and Brianza, Italy*

Laura Castoldi − *STMicroelectronics, Agrate Brianza 20864, Monza and Brianza, Italy*

Marinella Levi − *Department of Chemistry, Materials and Chemical Engineering "Giulio Natta", Politecnico di Milano, Milan 20133, Italy*

Complete contact information is available at: https://pubs.acs.org/10.1021/acsomega.1c01488

https://doi.org/10.1021/acsomega.1c01488
ACS Omega 2021, 6, 15892−15902

Author Contributions

The manuscript was written through the contributions of all authors. All authors have approved the final version of the manuscript.

Notes

The authors declare no competing financial interest.

■ ACKNOWLEDGMENTS

The authors acknowledge funding from STMicroelectronics.

■ REFERENCES

(1) Woehrmann, M.; Toepper, M. Polymerization of Thin Film Polymers. In *New Polymers for Special Applications*; De Souza Gomes, A., Ed.; InTech, 2012. DOI: 10.5772/48205.
(2) Li, Q.; Chen, L.; Gadinski, M. R.; Zhang, S.; Zhang, G.; Li, H. U.; Iagodkine, E.; Haque, A.; Chen, L.-Q.; Jackson, T. N.; Wang, Q. Flexible High-Temperature Dielectric Materials from Polymer Nanocomposites. *Nature* **2015**, *523*, 576−579.
(3) Ahmad, Z. Polymer Dielectric Materials. In *Dielectric Materials*; IntechOpen, 2012; pp 3−21.
(4) Mills, M. E.; Townsend, P.; Castillo, D.; Martin, S.; Achen, A. Benzocyclobutene (DVS-BCB) Polymer as an Interlayer Dielectric (ILD) Material. *Microelectron. Eng.* **1997**, *33*, 327−334.
(5) Gracias, A.; Tokranova, N.; Thelen, B. C. M.; Castracane, J. Influence of Diamond Nanoparticles on the Thermal Properties of Benzocyclobutene (BCB). *Phys. Status Solidi A* **2011**, *208*, 684−690.
(6) Zoschke, K.; Wolf, J.; Ehrmann, O.; Toepper, M.; Reichl, H. Copper/Benzocyclobutene Multi Layer Wiring-A Flexible Base Technology for Wafer Level Integration of Passive Components. *2007 9th Electronics Packaging Technology Conference*; IEEE, 2007, pp 295−302.
(7) Yang, J.; Cheng, Y.; Jin, Y.; Xiao, F. Synthesis and Properties of Novel Benzocyclobutene-Functionalized Siloxane Thermosets. *Polym. Int.* **2013**, *62*, 1684−1691.
(8) Yang, J.; Sun, M.; Cheng, Y.; Xiao, F. Study of Benzocyclobutene-Functionalized Siloxane Thermoset with a Cyclic Structure. In *2011 12th International Conference on Electronic Packaging Technology and High Density Packaging*, 2011, pp 1−6. DOI: 10.1109/ICEPT.2011.6066841.
(9) Ivanović, N.; Marjanović, N.; Rakočević, Z.; Andrić, V.; Hadžić, B.; Vukanac, I.; Đurđević, I.; Srećković, M. Changes of Properties of Cured and Uncured Disiloxane Bisbenzocyclobutene Thin Films under Irradiation. *Prog. Org. Coat.* **2013**, *76*, 257−262.
(10) Burdeaux, D.; Townsend, P.; Carr, J.; Garrou, P. Benzocyclobutene (BCB) Dielectrics for the Fabrication of High Density, Thin Film Multichip Modules. *J. Electron. Mater.* **1990**, *19*, 1357−1366.
(11) Niklaus, F.; Kumar, R. J.; McMahon, J. J.; Yu, J.; Lu, J.-Q.; Cale, T. S.; Gutmann, R. J. Adhesive Wafer Bonding Using Partially Cured Benzocyclobutene for Three-Dimensional Integration. *J. Electrochem. Soc.* **2006**, *153*, G291−G295.
(12) Bu, F.; Ma, Q.; Wang, Z. Delamination of Bonding Interface between Benzocyclobutene (BCB) and Silicon Dioxide/Silicon Nitride. *Microelectron. Reliab.* **2016**, *65*, 225−233.
(13) Niklaus, F.; Lu, J.-Q. Polymer Adhesive Wafer Bonding. In *Handbook of Wafer Bonding*; John Wiley & Sons, Ltd, 2012, pp 33−61. DOI: 10.1002/9783527644223.ch3.
(14) Marrion, A. *The Chemistry and Physics of Coatings*; Royal Society of Chemistry, 2004.
(15) Teraoka, I.; Solutions, P. *An Introduction to Physical Properties*; Wiley-Interscience, Electronic, 2002.
(16) Jabari, E.; Ahmed, F.; Liravi, F.; Secor, E. B.; Lin, L.; Toyserkani, E. 2D Printing of Graphene: A Review. *2D Mater.* **2019**, *6*, 042004.
(17) Na, J. Y.; Kang, B.; Lee, S. G.; Cho, K.; Park, Y. D. Surface-Mediated Solidification of a Semiconducting Polymer during Time-Controlled Spin-Coating. *ACS Appl. Mater. Interfaces* **2017**, *9*, 9871−9879.
(18) Norrman, K.; Ghanbari-Siahkali, A.; Larsen, N. B. 6 Studies of Spin-Coated Polymer Films. *Annu. Rep. Prog. Chem., Sect. C: Phys. Chem.* **2005**, *101*, 174−201.
(19) Sahu, N.; Parija, B.; Panigrahi, S. Fundamental Understanding and Modeling of Spin Coating Process: A Review. *Indian J. Phys.* **2009**, *83*, 493−502.
(20) Kelly, K. D.; Schlenoff, J. B. Spin-Coated Polyelectrolyte Coacervate Films. *ACS Appl. Mater. Interfaces* **2015**, *7*, 13980−13986.
(21) Sajedi-Moghaddam, A.; Rahmanian, E.; Naseri, N. Inkjet-Printing Technology for Supercapacitor Application: Current State and Perspectives. *ACS Appl. Mater. Interfaces* **2020**, *12*, 34487−34504.
(22) Guo, Y.; Patanwala, H. S.; Bognet, B.; Ma, A. W. K. Inkjet and Inkjet-Based 3D Printing: Connecting Fluid Properties and Printing Performance. *Rapid Prototyp. J.* **2017**, *23*, 562−576.
(23) Nayak, L.; Mohanty, S.; Nayak, S. K.; Ramadoss, A. A Review on Inkjet Printing of Nanoparticle Inks for Flexible Electronics. *J. Mater. Chem. C* **2019**, *7*, 8771−8795.
(24) Derby, B. Inkjet Printing of Functional and Structural Materials: Fluid Property Requirements, Feature Stability, and Resolution. *Annu. Rev. Mater. Res.* **2010**, *40*, 395−414.
(25) Martin, G. D.; Hutchings, I. M. Fundamentals of Inkjet Technology. In *Inkjet Technology for Digital Fabrication*; John Wiley & Sons, Ltd, 2014, pp 21−44. DOI: 10.1002/9781118452943.ch2.
(26) Derby, B. Additive Manufacture of Ceramics Components by Inkjet Printing. *Engineering* **2015**, *1*, 113−123.
(27) Choi, S.; Stassi, S.; Pisano, A. P.; Zohdi, T. I. Coffee-Ring Effect-Based Three Dimensional Patterning of Micro/Nanoparticle Assembly with a Single Droplet. *Langmuir* **2010**, *26*, 11690−11698.
(28) Dou, R.; Derby, B. Formation of Coffee Stains on Porous Surfaces. *Langmuir* **2012**, *28*, 5331−5338.
(29) Gorr, H. M.; Zueger, J. M.; Barnard, J. A. Characteristic Size for Onset of Coffee-Ring Effect in Evaporating Lysozyme-Water Solution Droplets. *J. Phys. Chem. B* **2012**, *116*, 12213−12220.
(30) Zhang, Z.; Zhang, X.; Xin, Z.; Deng, M.; Wen, Y.; Song, Y. Controlled Inkjetting of a Conductive Pattern of Silver Nanoparticles Based on the Coffee-Ring Effect. *Adv. Mater.* **2013**, *25*, 6714−6718.
(31) Shimoni, A.; Azoubel, S.; Magdassi, S. Inkjet printing of flexible high-performance carbon nanotube transparent conductive films by "coffee ring effect". *Nanoscale* **2014**, *6*, 11084−11089.
(32) Shen, X.; Ho, C.-M.; Wong, T.-S. Minimal Size of Coffee Ring Structure. *J. Phys. Chem. B* **2010**, *114*, 5269−5274.
(33) Li, Y.; Yang, Q.; Li, M.; Song, Y. Rate-Dependent Interface Capture beyond the Coffee-Ring Effect. *Sci. Rep.* **2016**, *6*, 24628.
(34) Al-Milaji, K. N.; Zhao, H. New Perspective of Mitigating the Coffee-Ring Effect: Interfacial Assembly. *J. Phys. Chem. C* **2019**, *123*, 12029−12041.
(35) Mampallil, D.; Eral, H. B. A Review on Suppression and Utilization of the Coffee-Ring Effect. *Adv. Colloid Interface Sci.* **2018**, *252*, 38−54.
(36) Sun, J.; Bao, B.; He, M.; Zhou, H.; Song, Y. Recent Advances in Controlling the Depositing Morphologies of Inkjet Droplets. *ACS Appl. Mater. Interfaces* **2015**, *7*, 28086−28099.
(37) Cui, L.; Zhang, J.; Zhang, X.; Huang, L.; Wang, Z.; Li, Y.; Gao, H.; Zhu, S.; Wang, T.; Yang, B. Suppression of the Coffee Ring Effect by Hydrosoluble Polymer Additives. *ACS Appl. Mater. Interfaces* **2012**, *4*, 2775−2780.
(38) Talbot, E.; Bain, C.; De Dier, R.; Sempels, W.; Vermant, J. Droplets Drying on Surfaces. In *Fundamentals of Inkjet Printing*; John Wiley & Sons, Ltd, 2015, pp 251−280. DOI: 10.1002/9783527684724.ch10.
(39) Yunker, P. J.; Still, T.; Lohr, M. A.; Yodh, A. G. Suppression of the Coffee-Ring Effect by Shape-Dependent Capillary Interactions. *Nature* **2011**, *476*, 308−311.
(40) He, P.; Derby, B. Controlling Coffee Ring Formation during Drying of Inkjet Printed 2D Inks. *Adv. Mater. Interfaces* **2017**, *4*, 1700944.
(41) Soltman, D.; Subramanian, V. Inkjet-Printed Line Morphologies and Temperature Control of the Coffee Ring Effect. *Langmuir* **2008**, *24*, 2224−2231.

https://doi.org/10.1021/acsomega.1c01488
ACS Omega 2021, 6, 15892−15902

(42) Sliz, R.; Czajkowski, J.; Fabritius, T. Taming the Coffee Ring Effect: Enhanced Thermal Control as a Method for Thin-Film Nanopatterning. *Langmuir* **2020**, *36*, 9562−9570.
(43) Seo, C.; Jang, D.; Chae, J.; Shin, S. Altering the Coffee-Ring Effect by Adding a Surfactant-like Viscous Polymer Solution. *Sci. Rep.* **2017**, *7*, 500.
(44) Chandramohan, A.; Dash, S.; Weibel, J. A.; Chen, X.; Garimella, S. V. Marangoni Convection in Evaporating Organic Liquid Droplets on a Nonwetting Substrate. *Langmuir* **2016**, *32*, 4729−4735.
(45) Bernasconi, R.; Angeli, M. C.; Mantica, F.; Carniani, D.; Magagnin, L. SU-8 Inkjet Patterning for Microfabrication. *Polymer* **2019**, *185*, 121933.
(46) Mikkonen, R.; Puistola, P.; Jönkkäri, I.; Mäntysalo, M. Inkjet Printable Polydimethylsiloxane for All-Inkjet-Printed Multilayered Soft Electrical Applications. *ACS Appl. Mater. Interfaces* **2020**, *12*, 11990−11997.
(47) Teichler, A.; Hölzer, S.; Nowotny, J.; Kretschmer, F.; Bader, C.; Perelaer, J.; Hager, M. D.; Hoeppener, S.; Schubert, U. S. Combinatorial Screening of Inkjet Printed Ternary Blends for Organic Photovoltaics: Absorption Behavior and Morphology. *ACS Comb. Sci.* **2013**, *15*, 410−418.
(48) Suntivich, R.; Shchepelina, O.; Choi, I.; Tsukruk, V. V. Inkjet-Assisted Layer-by-Layer Printing of Encapsulated Arrays. *ACS Appl. Mater. Interfaces* **2012**, *4*, 3102−3110.
(49) Robin, M.; Kuai, W.; Amela-Cortes, M.; Cordier, S.; Molard, Y.; Mohammed-Brahim, T.; Jacques, E.; Harnois, M. Epoxy Based Ink as Versatile Material for Inkjet-Printed Devices. *ACS Appl. Mater. Interfaces* **2015**, *7*, 21975−21984.
(50) Zhu, X.; Ng, L. W. T.; Hu, G.; Wu, T. C.; Um, D. S.; Macadam, N.; Hasan, T. Hexagonal Boron Nitride-Enhanced Optically Transparent Polymer Dielectric Inks for Printable Electronics. *Adv. Funct. Mater.* **2020**, *30*, 2002339.
(51) Liu, Q.; Le, M. Q.; Richard, C.; Liang, R.; Cottinet, P.-J.; Capsal, J.-F. Enhanced Pseudo-Piezoelectric Dynamic Force Sensors Based on Inkjet-Printed Electrostrictive Terpolymer. *Org. Electron.* **2019**, *67*, 259−271.
(52) Alamán, J.; López-Valdeolivas, M.; Alicante, R.; Peña, J.; Sánchez-Somolinos, C. Digital Luminescence Patterning via Inkjet Printing of a Photoacid Catalysed Organic-Inorganic Hybrid Formulation. *Polymers* **2019**, *11*, 430.
(53) Cho, C.-L.; Kao, H.-l.; Wu, Y.-H.; Chang, L.-C.; Cheng, C.-H. Direct Fabrication of Inkjet-Printed Dielectric Film for Metal-Insulator-Metal Capacitors. *J. Electron. Mater.* **2018**, *47*, 677−683.
(54) Du, Z.; Yu, X.; Han, Y. Inkjet Printing of Viscoelastic Polymer Inks. *Chin. Chem. Lett.* **2018**, *29*, 399−404.
(55) Tekin, E.; Smith, P. J.; Schubert, S. U. Inkjet Printing as a Deposition and Patterning Tool for Polymers and Inorganic Particles. *Soft Matter* **2008**, *4*, 703−713.
(56) Moon, S. J.; Robin, M.; Wenlin, K.; Yann, M.; Bae, B. S.; Mohammed-Brahim, T.; Jacques, E.; Harnois, M. Morphological Impact of Insulator on Inkjet-Printed Transistor. *Flexible Printed Electron.* **2017**, *2*, 035008.
(57) Graddage, N.; Chu, T.-Y.; Ding, H.; Py, C.; Dadvand, A.; Tao, Y. Inkjet Printed Thin and Uniform Dielectrics for Capacitors and Organic Thin Film Transistors Enabled by the Coffee Ring Effect. *Org. Electron.* **2016**, *29*, 114−119.
(58) Giannakou, P.; Tas, M. O.; Le Borgne, B.; Shkunov, M. Water-Transferred, Inkjet-Printed Supercapacitors toward Conformal and Epidermal Energy Storage. *ACS Appl. Mater. Interfaces* **2020**, *12*, 8456−8465.
(59) Herbert, R.; Lim, H.-R.; Yeo, W.-H. Printed, Soft, Nanostructured Strain Sensors for Monitoring of Structural Health and Human Physiology. *ACS Appl. Mater. Interfaces* **2020**, *12*, 25020−25030.
(60) Kang, Y. J.; Bail, R.; Lee, C. W.; Chin, B. D. Inkjet Printing of Mixed-Host Emitting Layer for Electrophosphorescent Organic Light-Emitting Diodes. *ACS Appl. Mater. Interfaces* **2019**, *11*, 21784−21794.
(61) Kang, B.; Lee, W. H.; Cho, K. Recent Advances in Organic Transistor Printing Processes. *ACS Appl. Mater. Interfaces* **2013**, *5*, 2302−2315.
(62) Hart, L. R.; Harries, J. L.; Greenland, B. W.; Colquhoun, H. M.; Hayes, W. Supramolecular Approach to New Inkjet Printing Inks. *ACS Appl. Mater. Interfaces* **2015**, *7*, 8906−8914.
(63) Miskiewicz, P.; Koch, M.; Walker, D.; Meyer, F.; Wieder, S.; Haley, J.; Dutta, V. InkJet Printing As Alternative Approach To Conventional Spin-on Material Coatings. In *2019 IEEE 21st Electronics Packaging Technology Conference (EPTC)*, 2019, pp 213−216. DOI: 10.1109/EPTC47984.2019.9026661.
(64) Roshanghias, A.; Ma, Y.; Gaumont, E.; Neumaier, L. Inkjet Printed Adhesives for Advanced M(O)EMS Packaging. *Flexible Printed Electron.* **2019**, *30*, 20285−20291.
(65) Hamad, E. M.; Bilatto, S. E. R.; Adly, N. Y.; Correa, D. S.; Wolfrum, B.; Offenhäusser, A.; Yakushenko, B.; Schöning, J. M. Inkjet Printing of UV-Curable Adhesive and Dielectric Inks for Microfluidic Devices. *Lab Chip* **2016**, *16*, 70−74.
(66) Hutchings, I. M.; Martin, G. D.; Hoath, S. D. *Fundamentals of Inkjet Printing*; John Wiley & Sons, Ltd, 2015, pp 1−12. DOI: 10.1002/9783527684724.ch1.Introductory Remarks
(67) Liu, Y.; Derby, B. Experimental Study of the Parameters for Stable Drop-on-Demand Inkjet Performance. *Phys. Fluids* **2019**, *31*, 032004.

https://doi.org/10.1021/acsomega.1c01488
ACS Omega 2021, 6, 15892−15902